7 Growth inhibition of established subcutaneous tumors in mice after intravenous administration of siRNA nanoparticles: Impact of tumor-specific targeting and dosing schedule

7.1 Abstract

As nanoparticle carriers for systemic in vivo delivery of small interfering RNA (siRNA) near clinical application, the design of suitable dosing schedules will become particularly important for their efficacy. This study addresses issues of practical relevance for siRNA nanoparticle delivery by measuring the impact of tumor-specific targeting and the effect of dose and dose frequency on the survival of mice bearing established subcutaneous tumors. We have previously shown that cyclodextrin-containing polycations (CDP) can form siRNA nanoparticles that exhibit desirable properties for in vivo application. Furthermore, we showed that these siRNA nanoparticles could inhibit tumor formation in mice when they were injected twice-weekly beginning immediately after the initial injection of tumor cells in a metastatic cancer model. A major challenge for tumor-targeted siRNA nanoparticle delivery is to inhibit tumor growth in established tumors, where issues such as tumor penetration and interactions in the tumor microenvironment can become critical factors governing efficacy. Here, we form syngeneic subcutaneous tumors using the Neuro2A neuroblastoma cell line. Three consecutive daily doses of Tf-targeted nanoparticles carrying 2.5 mg/kg of two different siRNA sequences targeting ribonucleotide reductase subunit M2 (RRM2) slow the growth of tumors that are ~100 mm^3 at the beginning of treatment; non-targeted nanoparticles are significantly less effective when given at the

same dose. Furthermore, administration of the three doses on consecutive days or every three days does not lead to statistically significant differences in tumor growth delay. Mathematical model calculations of siRNA-mediated target protein knockdown and tumor growth inhibition are used to elucidate possible mechanisms to explain the observed effects and provide guidelines for designing more effective siRNA-based treatment regimens.

7.2 Introduction

Delivery of a therapeutic agent to a desired site in the body after intravenous administration often remains the rate-limiting step in the development of novel therapeutic entities. Success hinges upon the ability to finely tune the properties of the therapeutic entity so that it can achieve efficacy at the target site at acceptable administered doses without inducing unacceptable toxic side effects. Small interfering RNA (siRNA) molecules are no exception, as safe and effective systemic delivery remains a major challenge impeding their widespread translation into the clinic (1).

siRNAs, which are double-stranded nucleic acids approximately 19-21 bp in length, are the effectors of RNA interference (RNAi), a naturally occurring mechanism for post-transcriptional gene silencing (2,3). These siRNAs find their cognate mRNAs through Watson-Crick base pairing and subsequently trigger the degradation of these target mRNAs. The effect of the mRNA degradation is a reduction in protein expression, and this mechanism can be exploited therapeutically to inhibit the expression of disease-associated targets such as ribonucleotide reductase (RNR). RNR is an attractive target for cancer therapies since it catalyzes the reduction of ribonucleotides into deoxyribonucleotides necessary for DNA replication and repair. Several potent siRNA

inhibitors of the M2 subunit of RNR (RRM2) have been identified, and these siRNAs have demonstrated the ability to inhibit the growth of tumor cell lines after transfection in vitro and transplantation into mice (4). A recent study by Avolio et al. demonstrated the in vitro and in vivo efficacy of an siRNA targeting ribonucleotide reductase (5). However, the dearth of suitable methods for in vivo siRNA delivery to tumors has yet limited translation of siRNAs for cancer therapy into the clinic.

Several promising strategies are currently being developed to specifically address systemic siRNA delivery. Covalent attachment of antibodies or cholesterol to the siRNAs can improve their pharmacokinetics and tissue distribution, addressing the problem of rapid renal clearance of naked siRNAs (6,7). Nanoparticle-based delivery vehicles also can improve the pharmacokinetics and tissue distribution of the delivered siRNAs, while providing additional properties such as large payload capacity and tunable surface modification. Stable nucleic acid lipid particles (SNALP) have been shown to deliver functional siRNA to the livers of mice and non-human primates leading to downregulation of *APOB* with good tolerability and minimal toxicity (8). These are non-targeted nanoparticles that passively accumulate in the liver and release their siRNA payload for uptake by the liver hepatocytes. Targeted nanoparticles attempt to enhance the uptake by certain cell populations through interactions with specific cell-surface receptors (9). For example, we have previously described a nanoparticle carrier based on cyclodextrin-containing polycations (CDP) that can be modified with transferrin-targeting ligands, and this system has shown efficacy in delivering functional siRNA to tumors in vivo (10-12).

In the study presented here, we examine the effects of using a CDP-based nanoparticle carrier to deliver therapeutic siRNAs at different dosing schedules to established subcutaneous tumors in mice. Tumor growth is followed by BLI and caliper measurements to measure changes in both cell viability and overall tumor burden. Mice are treated by low-pressure tail vein injection of the naked siRNAs or siRNA nanoparticles. Two different siRNAs targeting separate regions on RRM2 mRNA are shown to inhibit tumor cell growth in vitro and in vivo, while both an irrelevant control and a mismatched variant of one of the potent siRNAs do not show growth inhibition. Comparison of Tf-targeted and non-targeted nanoparticles as well as different dosing regimens is used to address practical considerations concerning optimal treatment design. Mathematical model calculations are used to provide possible explanations for the observed effects and to raise important issues for consideration when designing treatment regimens especially for cancer therapies that act through a cytostatic mechanism.

7.3 Materials and methods

7.3.1 siRNA duplexes

The sequences for the siRNA duplexes targeting the RRM2 gene (siR2A+5, siR2B+5, siR2B+6) have been previously described (4). siLuc is designed to target the firefly luciferase gene. These siRNAs were purchased as unmodified RNA duplexes from Integrated DNA Technologies. siCON is an unmodified siRNA bioinformatically designed to minimize the potential for targeting any human or mouse genes, and it was purchased as an RNA duplex from Dharmacon.

siR2A+5:

```
sense:      5′- CGAGUACCAUGAUAUCUGGCA –3′
antisense:  5′- CCAGAUAUCAUGGUACUCGAU -3′
```

siR2B+5:

```
sense:      5′- GAUUUAGCCAAGAAGUUCAGA –3′
antisense:  5′- UGAACUUCUUGGCUAAAUCGC -3′
```

siR2B+6:

```
sense:      5′- AUUUAGCCAAGAAGUUCAGAU –3′
antisense:  5′- CUGAACUUCUUGGCUAAAUCG -3′
```

siLuc:

```
sense:      5′- GUGCCAGAGUCCUUCGAUAdTdT –3′
antisense:  5′- UAUCGAAGGACUCUGGCACdTdT -3′
```

siCON:

```
sense:      5′- UAGCGACUAAACACAUCAAUU –3′
antisense:  5′- UUGAUGUGUUUAGUCGCUAUU -3′
```

7.3.2 In vitro transfection

Neuro2A-Luc cells with constitutive luciferase expression were seeded at $2x10^4$ cells per well in 24-well plates 2 days prior to transfection and grown in DMEM supplemented with 10% FBS and antibiotics (penicillin/streptomycin). siRNA was complexed with Oligofectamine (Invitrogen) according to manufacturer's instructions and 20 pmol siRNA was applied to each well in a total volume of 200 μL Opti-MEM I (Invitrogen). Transfection media was removed and replaced with complete media after 4 h. The kinetics of the luciferase knockdown were determined using the Xenogen IVIS 100 (Xenogen, Alameda, CA) as described previously (12). After the final time point, phase contrast images of the cells were taken using a Sony CCD-IRIS/RGB video camera attached to a Nikon Eclipse TE-300 inverted microscope.

7.3.3 Nanoparticle formation

Before addition to the nucleic acid, the CDP was mixed with adamantane (AD)-polyethylene glycol (PEG) at a 1:1 AD-PEG:β-CD (mol:mol) ratio in water. Targeted nanoparticles contained AD-PEG-transferrin (AD-PEG-Tf) as a percentage of the total AD-PEG in the mixture. For example, 1 mol% AD-PEG-Tf nanoparticles contained 0.01 moles AD-PEG-Tf for every 0.99 moles AD-PEG, and 0.1 wt% AD-PEG-Tf nanoparticles contained 0.001 g of AD-PEG-Tf for every 1 g of AD-PEG. The mixture of CDP, AD-PEG, and AD-PEG-Tf in water was then added to an equal volume of siRNA in water such that the ratio of positive charges from CDP to negative charges from the nucleic acid was equal to the desired charge ratio of 3 (+/-). An equal volume of 10% (w/v) glucose in water was added to the resulting nanoparticles to give a final concentration of 5% (w/v) glucose suitable for injection.

7.3.4 Dynamic light scattering (DLS)

Nanoparticle formulations were diluted to a volume of ~1.5 mL, placed in a cuvette, and inserted into a ZetaPALS (Brookhaven Instruments Corporation) instrument to measure both the size and zeta potential. Reported effective hydrodynamic diameters and zeta potentials represent the average values from a total of 10 runs each.

7.3.5 Animals and tumor formation

Female A/J mice were ordered from Jackson Laboratories. All tumor growth studies were performed when mice were 7-9 weeks old. Neuro2A-Luc cells were grown in DMEM supplemented with 10% FBS and antibiotics (penicillin/streptomycin) and subsequently trypsinized and resuspended in serum-free DMEM for injection. Each mouse was injected with $1x10^6$ Neuro2A-Luc cells in the right flank to form a

subcutaneous tumor. Tumor growth was monitored by caliper measurements of tumor volume ($0.5 \times l \times w^2$) and bioluminescent imaging of total emitted ph/s from the tumor region of interest. Treatments were commenced when the tumors had reached approximately 100 mm^3.

7.3.6 Intravenous administration of siRNA formulations

Naked siRNA or siRNA nanoparticles were mixed with an equal volume of 10% (w/v) glucose in water to yield a 5% (w/v) glucose (D5W) carrier solution suitable for injection. Each mouse was injected via lateral tail vein with 0.2 mL of the formulation in a 5% glucose solution.

7.3.7 Bioluminescent imaging (BLI)

Cell culture plates or mice were imaged using the Xenogen IVIS 100 imaging system (Xenogen). D-luciferin (Xenogen) was dissolved in PBS at 15 g L^{-1}. For in vitro assays in 24-well plates, 50 μL of the 15 g L^{-1} luciferin solution was added to each well containing 1 mL of media. Light emission was measured 2-3 minutes after addition of the luciferin. For in vivo experiments, 0.2 mL of the 15 g L^{-1} luciferin solution was injected i.p. 10 minutes before measuring the light emission. Mice were anesthetized with an initial dose of 5% isoflurane followed by a maintenance dose of 2.5% isoflurane. Bioluminescent signals were quantified using Living Image software (Xenogen).

7.3.8 Histology and confocal immunofluorescence microscopy

A/J mice bearing subcutaneous Neuro2A-Luc tumors were injected via tail vein with Tf-targeted nanoparticles carrying 2.5 mg/kg Cy3-siLuc. 18 h after injection, the mice were euthanized and the tumors were harvested, immediately placed in OCT

(TissueTek), and frozen on dry ice. Samples were stored at -80°C until sectioning. 5-µm thick cryosections were stained with hematoxylin and eosin (H&E) for histological analysis. To prepare for immunofluorescence staining, 5-µm thick cryosections were thawed and then fixed with acetone at -20°C for 15 min. Fixed cryosections were blocked with normal donkey serum (Jackson ImmunoResearch) for 1 h at room temperature, washed with PBS, and then placed in a humidity chamber for incubation with the primary antibodies in PBS + 1% BSA for 2 h at room temperature. A rat anti-mouse CD31 primary mAb (Pharmingen) was used at a dilution of 1:25, and a goat anti-luciferase primary pAb (Promega) was used at a dilution of 1:50. After washing with PBS, the cryosections were placed in a humidity chamber for incubation with the secondary antibodies in PBS for 1 h at room temperature. An AF488-conjugated donkey anti-rat secondary antibody (Invitrogen) was used at a dilution of 1:200, and a Cy5-conjugated donkey anti-goat secondary antibody (Jackson ImmunoResearch) was used at a dilution of 1:200. After washing with PBS, the slides were mounted using Biomeda Gel/Mount. Confocal microscopy was performed using a Zeiss LSM 510 Meta laser-scanning confocal microscope.

7.3.9 Determination of treatment efficacy

Quantification of the relative efficacy of various treatments was accomplished by calculating the time for the tumor to reach a luciferase signal of $1x10^{10}$ ph/s or a volume of 1000 mm^3. To facilitate comparison between treatment groups, the growth curves for each group were time-shifted using linear regression of the log-transformed initial growth curves so that the value at day 7 (pre-injection) for each group was 100 mm^3 (or $1x10^9$ ph/s). The time to endpoint (TTE) was then calculated by linear regression of a log-

transformed growth curve created from the final time point and the three previous time points. Mice whose tumors never reached the end point size were assigned a TTE value equal to the final day of the study. Statistical significance of the difference in TTEs between treatment groups was assessed using log-rank tests with two-tailed *p* values. TTEs based on the luciferase signal endpoint of $1x10^{10}$ ph/s are designated "TTE luc."

7.3.10 Tolerability

Mouse body weight was determined every 2-3 days during the course of treatment. Acceptable toxicity for each treatment group was defined as a mean body weight loss of no less than 20% at any point during or after treatment.

7.3.11 Mathematical modeling

We added a cell death parameter to the mathematical model of siRNA-mediated gene silencing described previously to enable simulation of treatment with a therapeutic siRNA (12). The differential equation governing cell growth was modified so that the cell growth rate would be reduced by a factor of P/Po where P is defined as the target protein concentration and Po is defined as the initial steady-state protein concentration in the cell. The equation was also modified such that the growth rate would be reduced to 0 when P/Po is reduced below an arbitrary threshold of 0.5. No parameters were included to account for possible cell death in addition to reduction in growth rate; however, such modifications could be easily incorporated if knockdown of a certain target protein is known to directly induce cell death. Furthermore, no modifications were added to account for the length of time the target protein is reduced below the threshold of 0.5, although it could be imagined that this might be physiologically relevant. The protein degradation rate, *kdegprot*, was adjusted to reflect the RRM2 protein half-life of 6.3 h

(13). The extracellular elimination rate constant, *kelimec*, was adjusted to 0.06 h^{-1} since the observed stability of the siRNA particles when incubated in serum is approximately 11 h, as shown in Chapter 5. The *partition* parameter governing the amount of the injected dose that reaches the tumor was adjusted to $1.5x10^{-2}$. Finally, tumor growth was modeled with a logistic growth equation where the maximum number of cells was limited to 1000× the initial number of injected cells. The remaining parameters were left unchanged from those described previously (12).

7.4 Results

7.4.1 In vitro growth inhibition by siRNAs targeting RRM2

Demonstration of the efficacy and sequence-specificity of the siRNA duplexes was first performed in cultured Neuro2A-Luc cells. The luciferase expression of the Neuro2A-Luc cells was monitored longitudinally using the Xenogen live-cell imaging system. Our previous work has shown that the luciferase knockdown in the Neuro2A-Luc cells lasts approximately 1 week with the greatest knockdown occurring 1-2 days after transfection (12). However, a different situation is observed when siRNAs that inhibit cell growth are applied. Instead of being used to follow the changes in luciferase expression, BLI is used to noninvasively measure the relative growth rates of the luciferase-expressing cells. The results in Figure 7.1 show the relative growth rates of cells transfected with siR2A+5, siR2B+5, siR2B+6, and siCON, and a phase contrast image of the cells in each treatment group after the final time point is shown to confirm the growth inhibition. The sequences for siR2A+5 and siR2B+5 were chosen based on their ability to reduce RRM2 protein levels in vitro and their complete sequence homology to mouse and human RRM2 (4). Furthermore, they target two separate sites

on the RRM2 mRNA. The sequence for siR2B+6 displayed reduced potency for RRM2 protein reduction relative to siR2A+5 and siR2B+5, even though it shares nearly complete homology to the siR2B+5 sequence, indicating the highly specific nature of the RNAi mechanism (4). Finally, siCON served as an irrelevant control sequence. Consistent with the expected reductions in RRM2 protein levels, both siR2A+5 and siR2B+5 inhibit cell growth relative to siR2B+6 and siCON. At the final time point, a two-tailed Student's t-Test was used to assess the significance of the cell growth inhibition by each treatment group. The growth inhibition by siR2B+5 relative to all other treatment groups was highly significant ($p<0.005$), inhibition by siR2A+5 was highly significant ($p<0.005$) relative to siCON and not quite significant relative to siR2B+6 ($p=0.05$), and inhibition by siR2B+6 was not significant ($p>0.1$) relative to siCON.

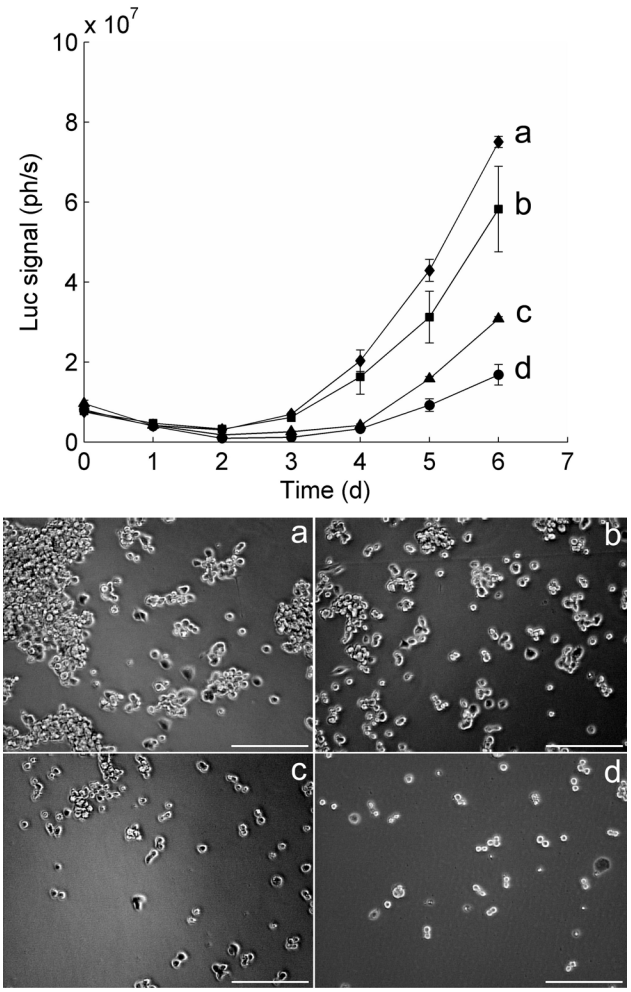

Figure 7.1. In vitro growth inhibition of Neuro2A-Luc cells after treatment with siCON (a), siR2B+6 (b), siR2A+5 (c), and siR2B+5 (d). Growth curves were measured for 6 consecutive days after treatment using live-cell bioluminescent imaging, and phase contrast images of cells from each of the four treatment groups were acquired after the final time point. The growth curves represent the mean luciferase signal from one (siR2A+5) or two (siR2B+5, siR2B+6, siCON) experiments with triplicate wells each. Error bars = *SE*.

7.4.2 Schedule dependence of tumor growth inhibition in vivo by siRNA nanoparticles

Based on the in vitro growth inhibition studies, siR2A+5 and siR2B+5 possess the capability to inhibit cell growth once they are internalized into the Neuro2A-Luc cells. When the siRNAs are administered intravenously in mice using the CDP-based nanoparticle carriers, however, only a small percent of the injected siRNA dose even reaches the tumor location, let alone is internalized by the target cells (as shown in

Chapter 5). Therefore, a systematic exploration of dose, dose frequency, and targeting ligand density was performed to determine what conditions may lead to sufficient delivery of the siRNAs into the Neuro2A-Luc tumor cells in mice to affect tumor growth rates.

Our previous work has shown that delivery of 2.5 mg/kg siRNA by the CDP-based nanoparticles was sufficient to achieve knockdown of a target gene in mouse tumors (11). Therefore, this dose was chosen as the initial dose for the investigations described here. The first set of experiments was conducted to determine the impact of dosing schedule. The rapid growth of the Neuro2A-Luc subcutaneous tumors provides the opportunity to conduct these experiments on a reasonable time scale, but it also limits the available dosing window since the length of time between the appearance of palpable tumors and their reaching the IACUC size limit is approximately 2 weeks. Figure 7.2 shows the effect of dosing schedules of qd×1, qd×3, or q3d×3 for doses of 2.5 mg/kg siRNA (siR2B+5 [n = 5], siR2B+6 [n = 5], and siCON [n = 4-5]) formulated into Tf-targeted (1 mol% Tf) nanoparticles. The data are represented as median luciferase signal (ph/s) measured by BLI. At all dosing schedules, siR2B+5 showed greater tumor growth inhibition than either siR2B+6 ($p<0.1$ for qd×1, $p<0.05$ for qd×3, and $p<0.1$ for q3d×3) or siCON ($p<0.1$ for qd×1, $p<0.15$ for qd×3, and $p<0.1$ for q3d×3). Although there was no statistically significant difference between the three dosing schedules of siR2B+5, the schedule of qd×3 (median TTE luc = 26.9 d) led to a greater delay in tumor growth relative to schedules of qd×1 (median TTE luc = 16.9 d) or q3d×3 (median TTE luc = 15.4 d). A single dose (qd×1) or three doses given every three days (q3d×3) yielded similar changes in the median tumor growth. The tumors may have grown to such a large

size by the time the last two doses of the q3d×3 schedule were given that the injected dose was unable to reach enough cells with an efficacious dose to impact tumor growth; therefore, this schedule had similar efficacy to a single dose. Three consecutive daily doses, however, may lead to sufficient siRNA accumulation at the tumor site and within the cells to have the desired impact on growth inhibition.

None of the treatments led to any overt signs of toxicity, and the mean body weight loss after treatment was ≤5% for all dosing schedules with siR2B+5, siR2B+6, and siCON. The body weight loss was transient with a maximum loss usually occurring within the 1-2 days immediately after treatment and a recovery to pre-treatment body weights thereafter.

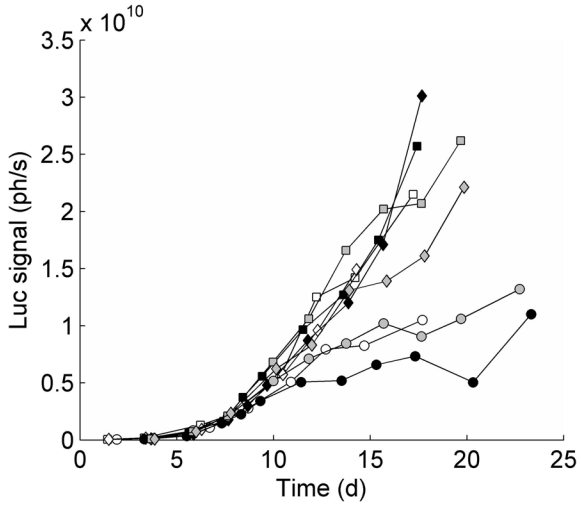

Figure 7.2. Effect of siRNA nanoparticle dosing schedule on the in vivo growth inhibition of established subcutaneous Neuro2A-Luc tumors in A/J mice. Tf-targeted nanoparticles containing 2.5 mg/kg of siR2B+5 (circles, n = 5), siR2B+6 (squares, n = 5), or siCON (diamonds, n = 4-5) were injected intravenously once (qd×1, white markers), on three consecutive days (qd×3, black markers), or once every three days (q3d×3, gray markers). Tumor growth was monitored by BLI, and the median luciferase signal is shown for each treatment group over the entire study period beginning with the initial injection of the cells. The first treatment was started around day 7 when the tumors achieved a luciferase signal of approximately $1x10^9$ ph/s (~100 mm^3).

7.4.3 Correlation between tumor bioluminescence (BLI) and tumor volume (caliper measurement)

One advantage of using a subcutaneous tumor model for these studies is that the tumor growth can be quantified by either BLI or caliper measurement of tumor volume. Since the goal of these studies was to examine the tumor growth inhibition by the delivered siRNAs, it was necessary to verify that the changes in luciferase expression correlated with changes in physical tumor volume. Tumor luciferase signal (ph/s) as a function of tumor volume (mm^3) is shown in Figure 7.3. These data represent the compilation of the luciferase signal and size measurements for several hundred tumors, since each data point represents the mean value for one of the treatment groups (typically n = 5) of mice at a given time after injection. The best fit ($r^2 = 0.89$) was obtained using a power law regression with an exponent of 0.9. This shows that BLI ph/s and caliper tumor volume are highly correlated, and there is nearly a linear correlation over 4 orders of magnitude. The accuracy of the correlation is highest for tumors with volumes >100 mm^3, an observation also made by Paroo et. al using a luciferase-expressing HeLa cell line (14). Furthermore, the correlation holds for mice treated with the therapeutic siRNAs, showing that treatment does not hinder the capability of BLI to follow changes in tumor volume in this tumor model. Consistent with our ex vivo analysis of the tumors in this study, Smrekar et al. observed very little necrosis in Neuro2A tumors. As necrotic regions could affect the correlation between luciferase signal and tumor volume, their minimal presence in the Neuro2A tumors may contribute to the good correlation observed in Figure 7.3.

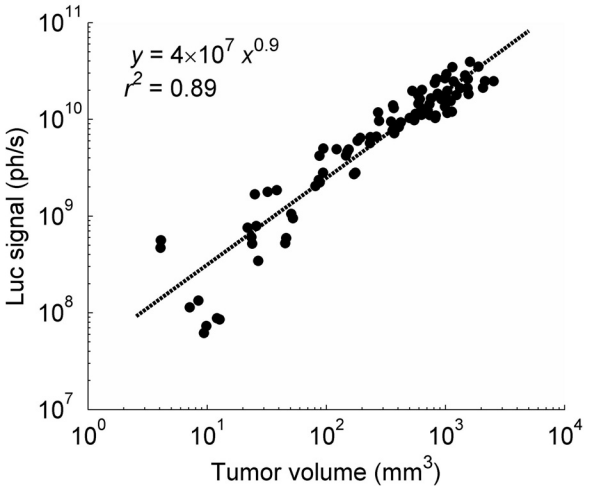

Figure 7.3. Correlation between tumor bioluminescence and tumor volume. Tumor luciferase signal (ph/s) as a function of tumor volume (mm^3) is shown for data from several hundred independent measurements (each data point represents the mean value for one of the treatment groups [n = 3-5] of mice at a given time after injection). The dashed line represents the power law regression line ($r^2 = 0.89$) that provided the best fit to the data.

However, a higher variability in bioluminescent imaging was observed compared to caliper measurements, especially when tracking the growth curves over time. Tumors (especially at early time points) which were placed deeper under the skin showed lower luciferase signal even though the physical size was identical to tumors located closer to the surface. BLI was therefore affected by variability in tissue penetration of light as well as differences between animals in luciferin injection and tumor uptake. Although both BLI and caliper measurements were still used to follow tumor growth in all of the experiments described here, the remaining results are reported as mean tumor volume (mm^3) owing to the reduced variability for caliper measurement of tumor volume. Notwithstanding, BLI can prove invaluable for tracking tumor growth in regions inaccessible to caliper measurement, such as sites of tumor metastasis, but such advantages are not apparent in a subcutaneous tumor model.

7.4.4 In vivo efficacy of naked siRNA vs. siRNA nanoparticles

The next set of experiments attempted to determine the effect of varying the siRNA formulation conditions while maintaining the qd×3 dosing schedule. The results in Figure 7.4A demonstrate the impact of variations in siRNA formulation conditions on the mean tumor volume, while the survival curves (time to 1000 mm^3) for each treatment group are shown in Figure 7.4B.

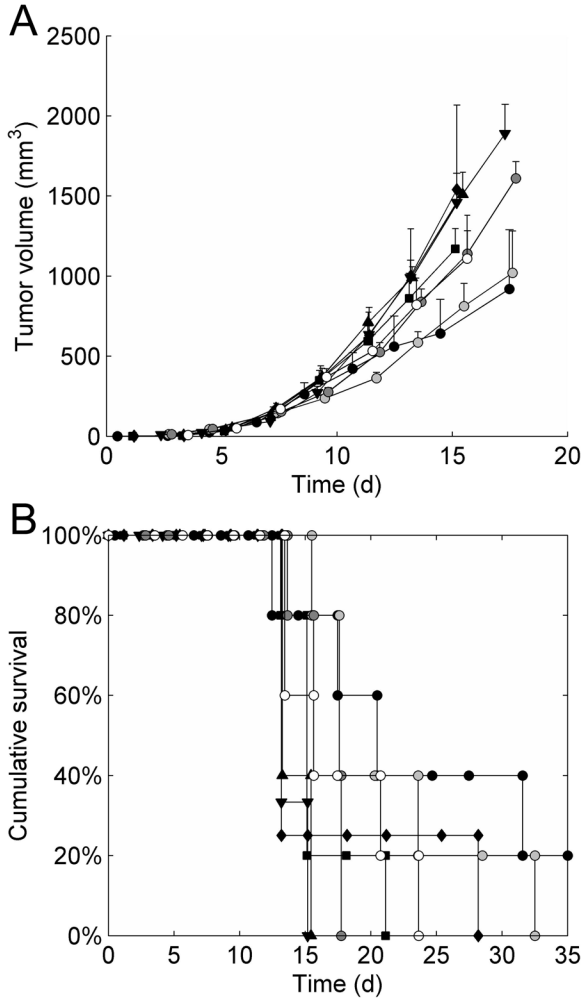

Figure 7.4. Effect of siRNA nanoparticle formulation on the in vivo growth inhibition of established subcutaneous Neuro2A-Luc tumors in A/J mice after intravenous injection of naked siRNA or siRNA nanoparticles for three consecutive days (qd×3). (A) Mean tumor volume. Error bars = *SE*. (B) Survival curves based on the endpoint of 1000 mm^3. Tf-targeted nanoparticles carrying 2.5 mg/kg of siR2B+5 were formulated without Tf targeting ligand (white circles, n = 5), with 0.1 wt% Tf (dark gray circles, n = 5), or with 1 mol% Tf (black circles, n = 5). Comparison is also made to Tf-targeted (1 mol%) nanoparticles carrying 5 mg/kg of siR2B+5 (light gray circles, n = 5), Tf-targeted (1 mol%) nanoparticles carrying 2.5 mg/kg of siR2B+6 (black squares, n = 5), Tf-targeted (1 mol%) nanoparticles carrying 2.5 mg/kg of siCON

(black diamonds, n = 4), 2.5 mg/kg of naked siR2B+5 (black triangles, n = 5), or no treatment (inverted black triangles, n = 3). The first treatment was started around day 7 when the tumors were ~100 mm^3.

Duxbury et al. reported that twice-weekly systemic administration of naked siRNA inhibited subcutaneous tumor growth in mice, and Avolio et al. showed subcutaneous tumor growth inhibition after thrice-weekly injection of naked siRNA (5,15). To test whether the same tumor growth inhibition was observed with naked siRNA as with the nanoparticle formulations in the Neuro2A subcutaneous tumor model studied here, 2.5 mg/kg of naked siR2B+5 (n = 5) was administered at the dosing schedule of qd×3 and the growth of tumors was followed over time. As with the nanoparticle formulations, the mice treated with naked siRNA showed a transient reduction in body weight ≤5%. The results in Figure 7.4 show that tumor growth in mice treated with naked siR2B+5 (median TTE = 12.9 d) was similar to that in untreated mice (n = 3, median TTE = 12.9 d). On the other hand, all treatments with the Tf-targeted nanoparticle formulations led to significant (p<0.05) changes in TTE relative to untreated mice or naked siR2B+5.

7.4.5 In vivo efficacy of targeted vs. non-targeted siRNA nanoparticles

Since the nanoparticle formulations appeared to be important for the efficacy of the delivered siRNA in the subcutaneous Neuro2A tumors, mice were treated with siR2B+5 at 2.5 mg/kg qd×3 formulated into nanoparticles containing 1 mol% Tf (n = 5), 0.1 wt% Tf (n = 5), or no Tf (non-targeted, n = 5) to assess the impact of Tf targeting ligand density. No adverse health events were observed after treatment with these formulations, and the transient body weight loss immediately after treatment was ≤5%. The data in Figure 7.4 indicate that nanoparticles with 1 mol% Tf were the most effective

for inhibiting tumor growth (median TTE = 17.6 d), while both non-targeted nanoparticles (median TTE = 15.7 d) and those with only 0.1 wt% Tf (median TTE = 15.0 d) showed less inhibition of tumor growth relative to untreated mice (median TTE = 12.9 d). However, both the 1 mol% Tf and 0.1 wt% Tf formulations showed a statistically significant ($p<0.05$) change in TTE relative to untreated mice, while the non-targeted formulation did not ($p>0.3$). The targeting ligand likely helps to enhance the intracellular uptake of the injected siRNA nanoparticles. In a metastatic xenograft model, we previously showed efficacy using Tf-targeted (0.1 wt%) siRNA nanoparticles (11). The greater efficacy observed here using the higher targeting ligand density (1 mol%) may reflect the reduced, but not negligible, affinity between the human Tf and the mouse TfR on mouse Neuro2A cells, or the use here of a subcutaneous instead of a metastatic tumor model. Further studies will be needed to optimize nanoparticle targeting ligand density, and the optimal density may depend on factors such as the cell line, tumor location, and tumor size.

Finally, mice were treated with the Tf-targeted (1 mol%) nanoparticles qd×3 with an siRNA dose of 5 mg/kg (n = 5). Treatment at the 5 mg/kg dose led to a transient decrease in mean body weight of ~11%, approximately twice that observed for formulations at 2.5 mg/kg; however, no other adverse health effects were observed. Relative to untreated mice, there was a highly significant change in TTE ($p<0.005$). However, as shown in Figure 7.4, there was no advantage for tumor growth inhibition with a dose of 5 mg/kg (median TTE = 15.9 d) relative to a dose of 2.5 mg/kg (median TTE = 17.6 d). This may indicate that the 2.5 mg/kg dose is sufficient to reduce the RRM2 protein levels below the value necessary to inhibit cell growth; therefore, if the

higher dose does not reach a higher percentage of the tumor cells, no phenotypic difference would be observed. It is possible that the nanoparticles may have restricted access to different cell populations within the tumor that inherently limit the efficacy of the delivered siRNA, although these important effects of intratumoral nanoparticle and siRNA distribution have yet to be extensively tested for this system.

7.4.6 Tumor growth inhibition in vivo correlates with in vitro cell growth inhibition

Although the siR2A+5, siR2B+5, siR2B+6, and siCON sequences had different effects on Neuro2A-Luc cell growth in vitro, it remained to be shown whether these same trends would be observed after nanoparticle-mediated delivery to subcutaneous Neuro2A-Luc tumors in vivo. The results in Figure 7.5 show the mean tumor volume (mm^3) for mice treated qd×3 with Tf-targeted (1 mol%) nanoparticles containing 2.5 mg/kg of siR2A+5 (n = 5), siR2B+5 (n = 5), siR2B+6 (n = 5), or siCON (n = 4). Corroborating the correlation between BLI and physical tumor volume presented in Figure 7.3, the trends for mean tumor volume are the same as for median tumor light output (ph/s) shown in Figure 7.2; however, Figure 7.5 also contains the data for mice treated with Tf-targeted nanoparticles containing siR2A+5. Like siR2B+5, the siR2A+5 sequence leads to significant tumor growth delay relative to untreated mice ($p<0.005$). In vivo tumor growth inhibition by the delivered siRNAs parallels their in vitro efficacy, with the potency of in vivo growth inhibition following the trend of siR2B+5 (median TTE = 17.6 d) > siR2A+5 (median TTE = 17.0 d) > siR2B+6 (median TTE = 14.3 d) > siCON (median TTE = 13.1).

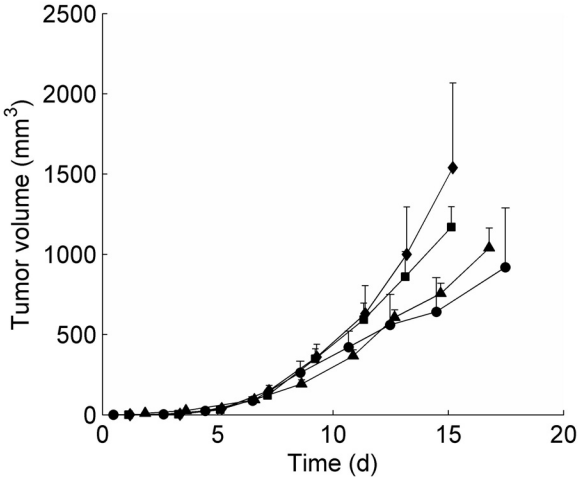

Figure 7.5. In vivo growth inhibition of established subcutaneous Neuro2A-Luc tumors in A/J mice after treatment with three independent sequences targeting RRM2 mRNA and an irrelevant control sequence. Tf-targeted (1 mol%) nanoparticles containing 2.5 mg/kg of siR2B+5 (circles), siR2B+6 (squares), siCON (diamonds), or siR2A+5 (triangles) were injected intravenously on three consecutive days (qd×3) once the tumors had reached a size of ~100 mm^3.

7.4.7 Histology and confocal immunofluorescence microscopy

To investigate the intratumoral distribution of siRNA after systemic delivery, H&E-staining and confocal immunofluorescence (IF) microscopy were used to examine cryosections of subcutaneous Neuro2A-Luc tumors excised from mice 18 h after tail-vein injection with Tf-targeted nanoparticles carrying 2.5 mg/kg Cy3-labeled siLuc (Figure 7.6). The H&E staining revealed the aggressive form of the Neuro2A-Luc tumors, characterized by densely packed tumor cells. However, IF staining for blood vessels using an anti-CD31 antibody showed that the tumors are also well-vascularized. This characteristic is particularly important to therapeutics that are applied intravenously and therefore require transport to the tumor through the blood vessels. Because of the extensive tumor vascularization, even intact nanoparticles that may have poor tissue penetration owing to their size (~70 nm) can potentially access a significant portion of the tumor cells. Cy3-labeled siLuc can be seen within the tumor cryosections in Figure 7.6,

although the intratumoral distribution of the siRNA molecules is highly heterogeneous. Moreover, IF-staining for luciferase expression within the tumor cryosections indicated a visible reduction in luciferase staining in the vicinity of the Cy3-labeled siLuc. This would be consistent with functional activity of the delivered Cy3-siLuc that is designed to inhibit luciferase expression. These results indicate that although the Tf-targeted nanoparticles can deliver functional siRNA to the subcutaneous Neuro2A-Luc tumors, their heterogeneous intratumoral distribution may limit the fraction of the tumor cells that can be treated (Figure 7.6B).

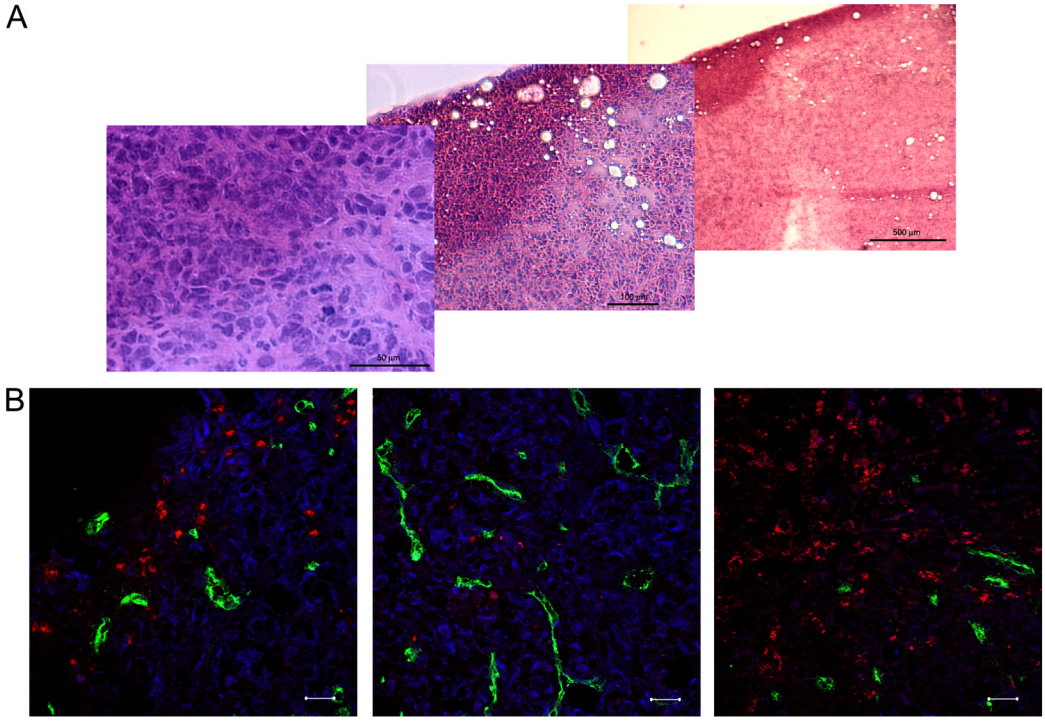

Figure 7.6. H&E staining (A) and confocal immunofluorescence microscopy (B) of Neuro2A-Luc tumor cryosections. Tumors were harvested 18 h after tail-vein injection of Tf-targeted nanoparticles containing Cy3-labeled siLuc (2.5 mg/kg). (A) H&E staining; images of the same tumor region are shown at 4X, 10X, and 40X magnification. (B) Confocal immunofluorescence microscopy of three different regions within the same tumor; green = anti-CD31, blue = anti-luciferase, red = Cy3-siLuc, and scale bar = 20 μm.

7.4.8 Mathematical model simulations and insights for siRNA-based treatment design

Based on our observations that a higher dose or a q3d×3 dosing schedule did not improve tumor growth inhibition, it may be that within the time frame of these experimental dosing schedules the nanoparticles essentially access the same region of tumor cells after each dose. Under such circumstances, there is no advantage to delivering more siRNA to the same region of cells once sufficient siRNA has been delivered to inhibit the growth of a given tumor cell. This is particularly important for therapeutic siRNAs which act to arrest cell growth or elicit cell death, since a threshold may exist beyond which further knockdown no longer achieves any advantage (i.e., the cell is already growth-arrested or dying). In these situations, multiple doses may not be needed for any given cell. On the other hand, multiple doses might be important if new cells are reached that either have not internalized any siRNA or have not internalized sufficient siRNA to pass beyond the threshold required for the phenotypic effect such as cell death. These concepts are illustrated in Figures 7.7 and 7.8 using a mathematical model to account for siRNA knockdown of a therapeutic target followed by cessation of cell growth if a threshold knockdown is achieved.

The duration of target knockdown after siRNA treatment is an important factor to consider when designing treatments. Figure 7.7 shows the expected duration of RRM2 protein knockdown after treatment (beginning on day 7) with 2.5 mg/kg qd×1 (I), 2.5 mg/kg q3d×3 (II), 2.5 mg/kg qd×3 (III), or 5 mg/kg qd×3 (IV). The only difference between Figures 7.8A and 7.8B is the rate of cell division of the tumor cells. In Figure 7.7A, the tumor cell doubling time is fixed at 1.5 d, so neither the maximum number of cells (logistic growth) nor target protein knockdown (even if the threshold knockdown is

surpassed) slow this growth. As expected, the knockdown lasts slightly longer than one week (12). In Figure 7.7B, however, the tumor cell growth rate is reduced as a result of target protein knockdown (proportional to relative protein level, P/Po), and growth is halted if $P/Po < 0.5$. Although the logistic growth equation is also applied in Figure 7.7B, it has a minimal impact on the expected protein knockdown in these simulations since removal of the maximum carrying capacity term does not significantly change the observed target knockdown curves. Therefore, these simulations demonstrate that the reduction in cell growth rate can lead to significantly longer target knockdown because of the reduced dilution from cell division. In the absence of cell division, target knockdown after siRNA delivery can last at least several weeks and even more than one month (8,12,16). This effect may represent a particularly important consideration in light of the increased use of cytostatic agents in oncology. If the treatment does not immediately induce cell death but rather slows or inhibits cell growth, then the siRNA-mediated target knockdown can persist for a substantial period after a single efficacious dose without the need for further dosing of the cells.

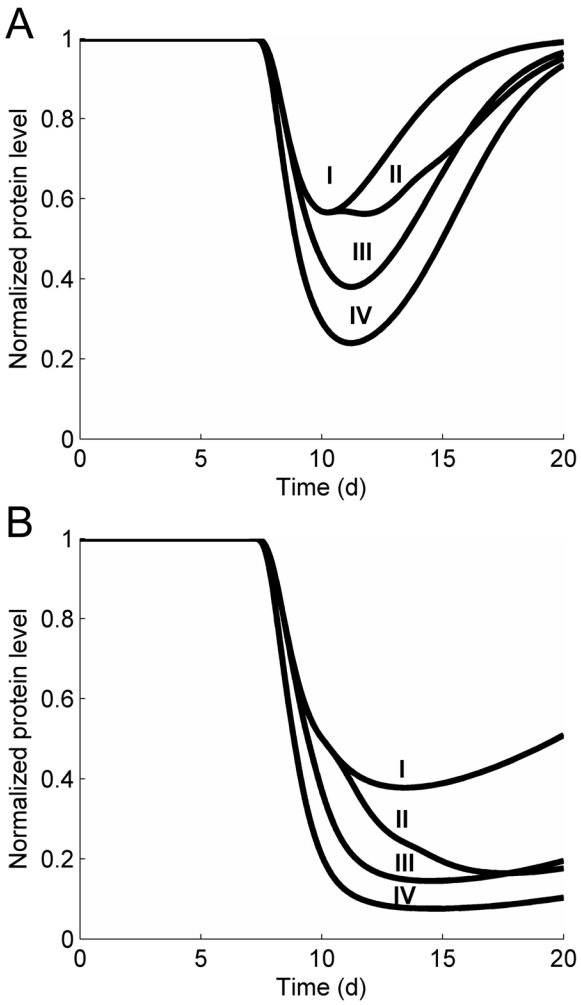

Figure 7.7. Model simulations showing the effect of tumor growth rate on the protein knockdown after siRNA nanoparticle treatment with dosing schedules of 2.5 mg/kg qd×1 (I), 2.5 mg/kg q3d×3 (II), 2.5 mg/kg qd×3 (III), or 5 mg/kg qd×3 (IV). (A) Protein knockdown in tumor cells with a constant doubling time of 1.5 d. (B) Protein knockdown in tumor cells with a growth rate that is slowed in proportion to protein knockdown and stopped once the protein knockdown passes the threshold of 50% protein knockdown.

The simulations in Figure 7.8 present an important caveat to the conclusions drawn from Figure 7.7. Although the target knockdown in any given cell may persist for a prolonged period if the tumor cell growth rate is reduced, it is highly unlikely that any treatment reaches all of the cells in the tumor, as illustrated by the heterogeneous intratumoral distribution of Cy3-siRNA shown in Figure 7.6. Particularly for relatively large therapeutic entities such as the siRNA nanoparticles, access to certain regions

within the tumor can be limited. Even if multiple doses are given, this does not ensure that new cells are reached within the tumor. In fact, Figure 7.8A shows what would happen if no new cells are reached even with subsequent doses. Treatment (beginning on day 7) with 2.5 mg/kg qd×1 (I), 2.5 mg/kg q3d×3 (II), 2.5 mg/kg qd×3 (III), or 5 mg/kg qd×3 (IV) all lead to essentially identical tumor growth inhibition. This is because the additional doses do not provide any therapeutic benefit since the target protein is already reduced below the threshold required for cessation of growth (Figure 7.7B). In such a situation where no new cells are reached with each treatment, multiple doses (or higher doses) will only be advantageous if additional reduction in target protein levels leads to further therapeutic benefit (i.e., a greater reduction in cell growth rate or induction of apoptosis at sufficiently low target protein levels).

For comparison, the simulations in Figure 7.8B assume that each additional dose reaches 50% new cells. After three doses, this predicts that there will be populations of cells that have been reached with a single dose, two doses, or all three doses. This ability to reach new cells leads to a greater total fraction of the tumor cells that receive therapeutic doses of the siRNA, and the benefit is clearly seen in Figure 7.8B. Under these conditions, the dosing schedules of 2.5 mg/kg qd×3 (III) or 5 mg/kg qd×3 (IV) are the most effective, owing to the faster reduction in target protein levels leading to cell growth inhibition. Because the tumor is growing rapidly, the number of cells to be reached increases with time. Therefore, if more cells need to be reached, then an equivalent total dose of siRNA may not be as effective in a large tumor as it is in a small tumor (if 50% of the total tumor cells are reached in each case). Alternatively, to achieve the same intracellular levels of siRNA in the larger tumor, a lower fraction of the total

tumor cells must be reached. Either scenario will lead to lower overall efficacy. The q3d×3 dosing schedule (II) in Figure 7.8B illustrates this point since the target protein levels in a portion of the cells that are reached at later time points are not reduced below the 50% threshold to stop cell growth.

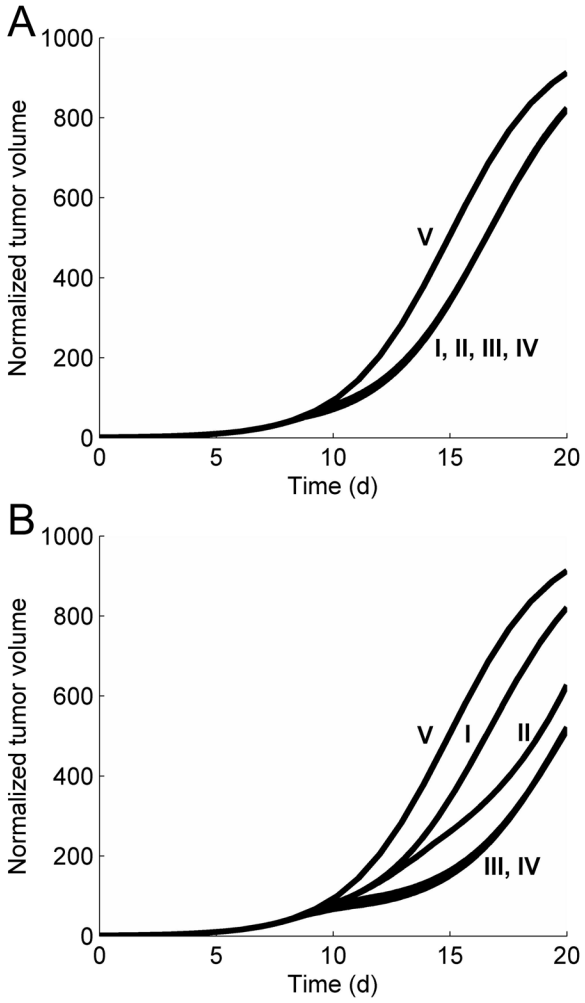

Figure 7.8. Model simulations comparing tumor growth inhibition after siRNA nanoparticle treatment in situations where (A) no new cells are reached or (B) 50% new cells are reached with each additional dose. Comparison is made between simulated siRNA nanoparticle treatment with dosing schedules of 2.5 mg/kg qd×1 (I), 2.5 mg/kg q3d×3 (II), 2.5 mg/kg qd×3 (III), or 5 mg/kg qd×3 (IV).

7.5 Discussion

In the present study, we demonstrated the ability of Tf-targeted siRNA nanoparticles to inhibit the growth of established subcutaneous Neuro2A tumors in a

syngeneic mouse model. The siRNAs were designed to target the M2 subunit of ribonucleotide reductase (RRM2), a crucial enzyme involved in preparing nucleotides for DNA replication (17). Three separate siRNAs targeting different regions on the RRM2 transcript were tested for their ability to inhibit the growth of Neuro2A-Luc (luciferase expressing) cells in vitro relative to cells transfected with an irrelevant control sequence (siCON). Consistent with previously reported RRM2 protein knockdown by these sequences, the order of potency for cell growth inhibition was siR2B+5 > siR2A+5 > siR2B+6 (4). While siR2A+5 and siR2B+5 target completely distinct regions in the RRM2 mRNA transcript, siR2B+5 and siR2B+6 are shifted by only 1 base pair. Moreover, siR2A+5 and siR2B+5 show complete homology to mouse RRM2 mRNA, but siR2B+6 contains a single mismatch at the last nucleotide of the target region in mouse RRM2 mRNA. These examples support the exquisite sensitivity of RNAi while also providing support that the observed effects are due to specific RRM2 protein knockdown.

These same trends in potency are observed in vivo after intravenous administration of Tf-targeted nanoparticles carrying the siRNAs. siRNA nanoparticle dosing schedules of 2.5 mg/kg qd×1, 2.5 mg/kg qd×3, and 2.5 mg/kg q3d×3 were compared, and the 2.5 mg/kg qd×3 led to the most pronounced growth inhibition. Increasing the siRNA dose to 5 mg/kg did not yield greater tumor growth inhibition. Importantly, non-targeted nanoparticles given at a dose of 2.5 mg/kg qd×3 were less effective at achieving tumor growth inhibition. Several groups have reported similar trends showing that inclusion of a targeting ligand is necessary for achieving therapeutic efficacy, most likely by enhancing the intracellular delivery of the nanoparticle payload (18,19).

A particular concern with siRNA-based therapies is the possibility of nonspecific effects, such as immune stimulation, that could mask the sequence-specific effects of the siRNA (20). Toxicity studies in cynomolgus monkeys have been conducted after intravenous administration of Tf-targeted nanoparticles formed using the CDP delivery vehicle and the siR2B+5 sequence at siRNA doses up to 27 mg/kg (21). At siRNA doses up to 9 mg/kg, the Tf-targeted nanoparticles were well-tolerated with no overt signs of toxicity; importantly, there was a lack of significant complement activation or immune response at these doses. This indicates that the efficacy observed here is not related to non-specific effects from immune stimulation.

These results provide several important insights into systemic siRNA delivery using nanoparticle formulations. According to the in vitro data shown in Figure 7.2, a single dose of siRNA can be sufficient to achieve the phenotypic effect of cell growth arrest, presumably because a single dose can inhibit the RRM2 target long enough so that the rapidly dividing cells will attempt to divide during the window of inhibition, triggering the growth arrest or even cell death. With targets that disrupt cell division, for example, prolonged inhibition in any cell may not be needed, so the criteria used to choose the dosing intervals should not be designed to necessarily prolong inhibition in a given cell. Instead, multiple doses should be designed to maximize the fraction of cells reached with a sufficient siRNA dose for efficacy. The surprising observation that a higher siRNA dose did not lead to greater tumor growth inhibition can possibly be explained by the threshold hypothesis illustrated by the simulations in Figures 7.7 and 7.8. Essentially, if the target is already knocked down sufficiently in a cell, and the higher dose does not reach any greater fraction of the total tumor cells, then giving a

higher dose will provide no therapeutic advantage. This effect is magnified by the prolonged duration of target knockdown expected if cell growth is inhibited after treatment. These criteria would not be expected to apply for other therapeutic applications, such as infectious diseases or metabolic disorders, where the target may have to be continuously repressed to achieve the therapeutic effect. In such applications, multiple dosing schedules must be designed to maintain the silencing within a given cell. As we showed previously, this dosing schedule will be largely governed by the doubling time of the target cell (12).

In conclusion, these studies address issues of practical relevance for siRNA nanoparticle delivery including the impact of tumor-specific targeting and the effect of dose and dose frequency. The results emphasize the importance of rationally designing dosing schedules based on the characteristics of the therapeutic target, since the duration of gene inhibition in a given cell required for therapeutic efficacy will vary. Compared to systemically delivered naked siRNA molecules, tumor-targeted siRNA nanoparticle formulations were shown to be significantly more effective in slowing the growth of subcutaneous tumors. This increased efficacy may be attributed at least partly to the capability of nanoparticles to deliver thousands of individual siRNA molecules per cellular uptake event, increasing the chance for therapeutic efficacy within a cell. Furthermore, targeted nanoparticles are shown to be more effective than non-targeted nanoparticles, indicating that inclusion of a targeting ligand may be critical for uptake by the desired cell population after localization to the tumor microenvironment. These results emphasize the need to incorporate both tumor-specific (e.g., accessibility, number of target cells, and growth rate) and treatment-specific (e.g., threshold knockdown

required, cytostatic vs. cytotoxic, and duration of therapeutic effect after a given dose) parameters into the design of siRNA-based treatments for cancer therapy.

7.6 Acknowledgments

This work was supported by an NSF Graduate Research Fellowship to D.W.B. and the NCI-supported Nanosystems Biology Cancer Center. The authors thank Sofia Loera (City of Hope) for performing the tissue sectioning and H&E staining, and Calando Pharmaceuticals for the gift of CDP, AD-PEG, and AD-PEG-Tf.

7.7 References

1. Behlke, M.A. (2006) Progress towards in vivo use of siRNAs. *Mol Ther*, **13,** 644-670.
2. Dykxhoorn, D.M., Palliser, D. and Lieberman, J. (2006) The silent treatment: siRNAs as small molecule drugs. *Gene Ther*, **13,** 541-552.
3. Elbashir, S.M., Harborth, J., Lendeckel, W., Yalcin, A., Weber, K. and Tuschl, T. (2001) Duplexes of 21-nucleotide RNAs mediate RNA interference in cultured mammalian cells. *Nature*, **411,** 494-498.
4. Heidel, J.D., Liu, J.Y.-C., Yen, Y., Zhou, B., Heale, B.S.E., Rossi, J.J., Bartlett, D.W. and Davis, M.E. (2007) Potent siRNA inhibitors of ribonucleotide reductase subunit RRM2 reduce cell proliferation in vitro and in vivo. *Clin Cancer Res*, **13,** 2207-2215.
5. Avolio, T.M., Yoon, L., Feng, N., Xiong, K., Jin, H., Wang, M., Vassilakos, A., Wright, J. and Young, A. (2007) RNA interference targeting the R2 subunit of ribonucleotide reductase inhibits growth of tumor cells in vitro and in vivo. *Anti-Cancer Drugs*, **18,** 377-388.
6. Song, E., Zhu, P., Lee, S.-K., Chowdhury, D., Kussman, S., Dykxhoorn, D.M., Feng, Y., Palliser, D., Weiner, D.B., Shankar, P. et al. (2005) Antibody mediated in vivo delivery of small interfering RNAs via cell-surface receptors. *Nat Biotechnol*, **23,** 709-717.
7. Soutschek, J., Akinc, A., Bramiage, B., Charisse, K., Constien, R., Donoghue, M., Elbashir, S., Geick, A., Hadwiger, P., Harborth, J. et al. (2004) Therapeutic silencing of an endogenous gene by systemic administration of modified siRNAs. *Nature*, **432,** 173-178.
8. Zimmermann, T.S., Lee, A.C.H., Akinc, A., Bramlage, B., Bumcrot, D., Fedoruk, M.N., Harborth, J., Heyes, J.A., Jeffs, L.B., John, M. et al. (2006) RNAi-mediated gene silencing in non-human primates. *Nature*, **441,** 111-114.
9. Schatzlein, A.G. (2003) Targeting of synthetic gene delivery systems. *J Biomed Biotechnol*, **2,** 149-158.
10. Bartlett, D.W. and Davis, M.E. (2007) Physicochemical and biological characterization of targeted, nucleic acid-containing nanoparticles. *Bioconjugate Chem*, **18,** 456-468.
11. Hu-Lieskovan, S., Heidel, J.D., Bartlett, D.W., Davis, M.E. and Triche, T.J. (2005) Sequence-specific knockdown of EWS-FLI1 by targeted, nonviral delivery of small interfering RNA inhibits tumor growth in a murine model of Ewing's sarcoma. *Cancer Res*, **65,** 8984-8992.
12. Bartlett, D.W. and Davis, M.E. (2006) Insights into the kinetics of siRNA-mediated gene silencing from live-cell and live-animal bioluminescent imaging. *Nucleic Acids Res*, **34,** 322-333.
13. Choy, B.K., McClarty, G.A., Chan, A.K., Thelander, L. and Wright, J.A. (1988) Molecular mechanisms of drug resistance involving ribonucleotide reductase: Hydroxyurea resistance in a series of clonally related mouse cell lines selected in the presence of increasing drug concentrations. *Cancer Res*, **48,** 2029-2035.

14. Paroo, Z., Bollinger, R., Braasch, D., Richer, E., Corey, D., Antich, P. and Mason, R. (2004) Validating bioluminescence imaging as a high-throughput, quantitative modality for assessing tumor burden. *Mol Imaging*, **3,** 117-124.
15. Duxbury, M.S., Matros, E., Ito, H., Zinner, M.J., Ashley, S.W. and Whang, E.E. (2004) Systemic siRNA-mediated gene silencing: a new approach to targeted therapy of cancer. *Ann Surg*, **240,** 667-676.
16. Bartlett, D.W. and Davis, M.E. (2007) Effect of siRNA nuclease stability on the in vitro and in vivo kinetics of siRNA-mediated gene silencing. *Biotechnol Bioeng***,** in press.
17. Cerqueira, N.M.F.S.A., Pereira, S., Fernandes, P.A. and Ramos, M.J. (2005) Overview of ribonucleotide reductase inhibitors: an appealing target in anti-tumour therapy. *Curr Med Chem*, **12,** 1283-1294.
18. Kirpotin, D.B., Drummond, D.C., Shao, Y., Shalaby, M.R., Hong, K., Nielsen, U.B., Marks, J.D., Benz, C.C. and Park, J.W. (2006) Antibody targeting of long-circulating lipidic nanoparticles does not increase tumor localization but does increase internalization in animal models. *Cancer Res*, **66,** 6732-6740.
19. Maeda, N., Miyazawa, S., Shimizu, K., Asai, T., Yonezawa, S., Kitazawa, S., Namba, Y., Tsukada, H. and Oku, N. (2006) Enhancement of anticancer activity in antineovascular therapy is based on the intratumoral distribution of the active targeting carrier for anticancer drugs. *Biol Pharm Bull*, **29,** 1936-1940.
20. Judge, A.D., Bola, G., Lee, A.C.H. and MacLachlan, I. (2006) Design of noninflammatory synthetic siRNA mediating potent gene silencing in vivo. *Mol Ther*, **13,** 494-505.
21. Heidel, J.D., Yu, Z., Liu, J.Y.-C., Rele, S.M., Liang, Y., Zeidan, R.K., Kornbrust, D.J. and Davis, M.E. (2007) Administration in non-human primates of escalating intravenous doses of targeted nanoparticles containing ribonucleotide reductase subunit M2 siRNA. *P Natl Acad Sci USA*, **104,** 5715-5721.